Characterization of Radio-Photo-Luminescence (RPL) Dosimeters as Radiation Monitors in the CERN Accelerator Complex

Dejan Pramberger, Ygor Q. Aguiar, *Member, IEEE*, Julia Trummer, and Helmut Vincke

***Abstract*— Dosimetry is a crucial activity in irradiation campaigns to qualify electronics and materials to operate in radiation environments. In addition, it also provides means of monitoring radiation levels in accelerator environments to prevent radiation damage to the machines and improve system lifetime. Therefore, this work provides the characterization of radio-photo-luminescence (RPL) glass dosimeters as a high-level radiation monitor to be used in the mixed radiation fields observed in CERN's accelerator environment as well as in irradiation campaigns for the qualification of electronic components and materials. Here, two methods to improve the measured dose are presented, one for the correction due to the fading of the RPL dosimeters (RPLDs), where an improvement of over 40% of the measured to the expected dose could be achieved, and one method that corrects the measured dose in mixed-particle fields to dose in water or air.**

***Index Terms*— Accelerator environment, dosimetry, radiation monitoring (RadMON), radio-photo-luminescence dosimeter (RPLD).**

I. Introduction

THE mixed radiation fields present in the accelerator complex at CERN can cause damage to materials and electronic components located along its tunnels and alcoves [1]. For instance, electronic circuits are subject to the total ionizing dose (TID) that changes the parametric characteristics of semiconductor devices leading to degraded performance or even their failure. The radiation environment in the Large Hadron Collider (LHC) complex is a product of the beam losses in the machines, resulting into a mixed-particle and energy radiation field. Therefore, to maximize machine availability and quantify the radiation damage, systematic radiation-level monitoring is highly important due to the distribution of different radiation fields depending on the location within the tunnels and alcoves of the accelerator. Based on the radiation sensitivity of the electronic components and materials, different radiation hardness assurance (RHA) approaches are applied to prevent catastrophic events induced by radiation damage. In this context, several monitoring systems have been developed and adopted at CERN, such as the beam loss monitor (BLM) system [2], radiation monitoring (RadMON) system [3], distributed optical fiber (OF) system [4], and also the support of Monte Carlo calculations using FLUKA [5]–[7]. Despite the good coverage and efficiency of these monitors, there is still a need for a compact monitor with a wide operation range that can be closely placed next to the equipment to measure ionizing dose reaching the MGy range as observed in the Super Proton Synchrotron (SPS) ring.

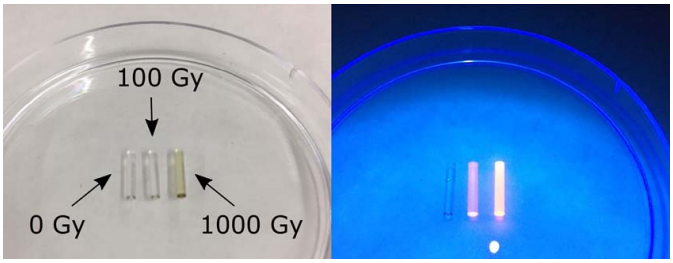

Fig. 1. FD7 glass RPLDs illuminated with visible light (left image) and UV-light (right image). Nonirradiated dosimeter (left) and irradiated dosimeter with absorbed dose of 100 Gy (center) and with absorbed dose of 1000 Gy (right). Orange luminescence light can be seen during exposure to UV light.

In this context, the radio-photo-luminescence dosimeters (RPLDs), although widely adopted in low-range applications (0.1 mGy–10 Gy [8]), can be used as monitors for accelerator environments with a broad range of particle fields. Furthermore, they are very small passive dosimeters, as shown in Fig. 1, which can easily be used next to the equipment without the need of any infrastructure such as cabling or power supply. Therefore, this work presents a high-level dosimetry system based on the RPLDs for the monitoring of radiation levels in the accelerator complex. One of the challenges of working in a mixed radiation field is that most of the radiation monitors are usually calibrated under radiation sources such as cobalt-60 (^{60}Co) or cesium-137 (^{137}Cs) radioisotopes. As a consequence, the measured dose must be interpreted as an equivalent dose under the calibration radiation field, which can significantly deviate from the actual absorbed dose from a given radiation field [9]. Accordingly, in this article, we propose a methodology to correct the measured dose for mixed-particle fields based on Monte Carlo calculations. Another challenge in dosimetry systems is the fading effects due to the long

Manuscript received 7 April 2022; revised 8 May 2022; accepted 10 May 2022. Date of publication 12 May 2022; date of current version 18 July 2022.

Dejan Pramberger, Julia Trummer, and Helmut Vincke are with the Radiation Protection Department, European Organization for Nuclear Research (CERN), CH-1211 Geneva 23, Switzerland (e-mail: dejan.pramberger@cern.ch).

Ygor Q. Aguiar is with the Accelerator Systems Department, European Organization for Nuclear Research (CERN), CH-1211 Geneva 23, Switzerland (e-mail: ygor.aguiar@cern.ch).

Color versions of one or more figures in this article are available at https://doi.org/10.1109/TNS.2022.3174784.

Digital Object Identifier 10.1109/TNS.2022.3174784

TABLE I

MATERIAL COMPOSITION OF THE FD7 GLASS ROD (GD-301) FROM CHIYODA TECHOL, JAPAN

	Density [g/cm^3]	O [wt-%]	P [wt-%]	Na [wt-%]	Al [wt-%]	Ag [wt-%]
FD7	2.6041	51.16	31.55	11.0	6.12	0.17

exposure and storage times [10]. Although the RPLDs have shown a fairly low fading rate [11], in this article, we have also presented the fading correction used in the framework of the RadMON activity at CERN [12].

This article is organized as follows. First, in Section II, the fundamental mechanisms behind the RPLDs and their calibration procedure to be used as a high-level dosimetry system are presented. In Section III, a methodology to obtain the corrected response of the dosimeter under a mixed radiation field is proposed. In addition, the fading effects related to the storage and long exposure times are discussed in Section IV. Finally, Sections V and VI provide the discussion of the results and the conclusions, respectively.

II. RADIO-PHOTO-LUMINESCENCE DOSIMETERS

In dosimetry, stimulated luminescence can be used to determine the total integrated dose by measuring the light emission intensity of a luminescent material [13]. The RPLDs are phosphate glasses doped with silver (Ag) impurities as it is a good activator ion for the RPL emission [10], [14]. When the dosimeters are exposed to ionizing radiation, the resulting electron–hole pairs are trapped at the extrinsic point defects introduced by the silver ions in the glass lattice and form defect centers. Therefore, the energy deposition and the corresponding efficiency of the dosimeter are proportional to the number of those centers. These dosimeters are well known for having very stable centers and low dose-rate dependence [10], [14]. In this work, FD7 glass rods (GD-301), with a material composition referenced in Table I, from Chiyoda Technol, Japan, are used, with a diameter of 0.15 cm and a length of 0.85 cm. The silver content in the FD7 material is at low level as concentration quenching can lead to a reduction in the dosimeter sensitivity [15].

The centers can be classified into two groups: luminescence centers (also known as RPL centers), responsible for the RPL light emission when excited by UV light, and color centers, responsible for an increasing coloration of the glass dosimeter with increasing dose and a consequent light absorption within the glass. The excitation of the RPL centers using UV light (365 nm) induces the emission of an orange luminescence light (610 nm), which is proportional to the absorbed dose. This effect can be seen in Fig. 1, where three dosimeters with absorbed doses of 0, 100, and 1000 Gy are illuminated with visible and with UV light. For low-dose applications up to around 300 Gy, a linear relationship can be observed between the RPL light and absorbed dose. However, an increase of color centers with increasing absorbed dose is responsible for an increase of photon absorption of the luminescence and UV light. This phenomenon leads to the flattening of the luminescence response curve around 1 kGy, which is shown in Fig. 2. Besides leading to high uncertainty in this

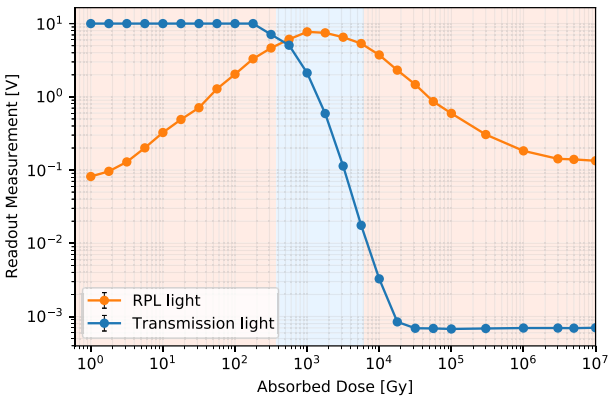

Fig. 2. Calibration curves for the RPL and transmission light measurement, measurement signal (V) versus reference absorbed dose (Gy). The dosimeters were calibrated in a ^{60}Co gamma field in the Risø HDRL Facility, Denmark [17].

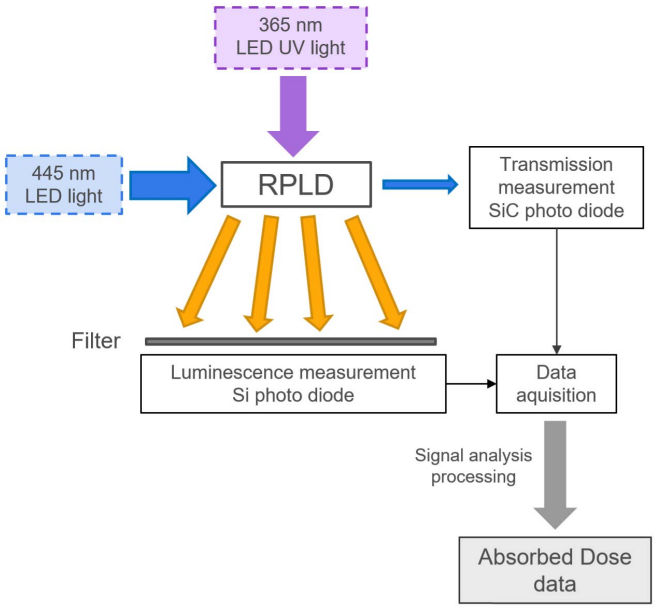

Fig. 3. Diagram of the RPL readout system developed and patented at CERN [18]. Two LED light sources are used to excite the RPL centers and measure the luminescence light and transmission light intensities.

dose range, one RPL signal value can correspond to two dose values: one in the lower dose range and one in the higher dose range. Accordingly, conventional applications of RPLDs are limited to low-level radiation environments such as personal dosimetry in medical applications [10]. To extend the applicability of such a dosimetry system, a two-light measurement methodology shown in Fig. 3 was developed at CERN [14], [16] to quantify not only the luminescence emission but also the photon absorption in the color centers. Therefore, for the readout measurements, besides exposure to UV light, the RPLDs are also exposed to a light transmission measurement where blue light with a wavelength of 445 nm is used. The light beam is directed onto the front face of the dosimeter and the attenuated light is measured at its back face by a SiC photodiode. Based on the measurement of the intensity of the luminescence and transmission lights, the absorbed dose data can be extracted from the dosimeters. The uncertainty of the readout measurement is about 5% (1σ).

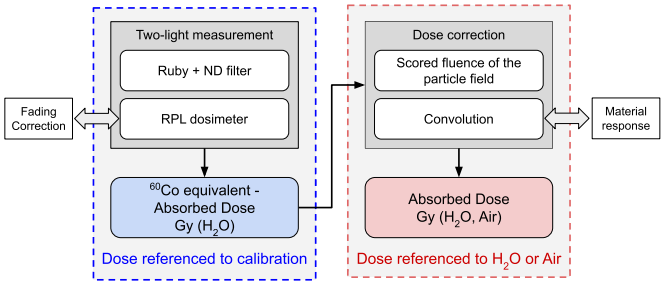

Fig. 4. Simplified block diagram of the RPL dosimetry system used at CERN.

As previously mentioned, for low doses, the dosimeter is still transparent and no significant attenuation is observed in the RPL signal until around 300 Gy. Therefore, the dose can be easily estimated from the RPL signal measurement. However, as clearly shown in Fig. 2, in the intermediate dose range where a flattening of the RPL light signal can be observed, the transmission light signal is used as the reference signal for the measurement. In addition, this signal is also used to identify if a given RPL signal corresponds to a low-dose value (high transmission signal) or to a high-dose value (low transmission signal). Based on the two-light measurement methodology, the RPLs can be used up to the MGy range of application.

Finally, some dose-rate effects might be encountered due to the accelerated irradiation used in the calibration campaign (from 188 Gy/h to 4.7 kGy/h). In our preliminary studies, an underestimation was observed when the standard accelerated calibration curve is adopted, in which a higher impact can be expected for the low-dose range up to about 1 kGy. Although this study is still under development and it goes beyond the scope of this manuscript, a very good agreement was observed when the RPLDs were benchmarked with different radiation monitors used in the accelerator as, for example, silica-based OFs and ionization chambers (BLMs).

III. Response to Mixed-Particle Field

The recorded calibration curves in Fig. 2 are achieved by the measurement of RPLDs irradiated in a ^{60}Co gamma field (Risø HDRL Facility, Denmark [17]) referenced to dose to water. For this reason, the dose received by a dosimeter that was irradiated in an arbitrary radiation field must be interpreted as dose of ^{60}Co, which causes the same effect in the dosimeter. As a consequence of the difference of the calibration field to the mixed high-energy fields present in the accelerator complex at CERN, the measured dose can deviate significantly from the actual absorbed dose. Based on previous attempts [9], a procedure was found [19] to transform the measured dose result, caused by a given arbitrary mixed-particle field, to dose to water or air. As a result, this approach can be utilized for known fluences of the radiation fields as described in Fig. 4 to correct the measured dose. This approach utilizes the response of the involved materials to the calibration field and the radiation field present during irradiation of the dosimeter to achieve the correction. The response $\overline{R}$ in units of Gy $\cdot$ cm^2 of a material can be understood as the absorbed dose deposited per unit fluence in the reference material by a particle p with an energy E. This value can be simulated by use of the particle Monte Carlo code FLUKA. In order to generalize the approach, a mean response is introduced to account for all particles and energies present in the relevant radiation fields. With this mean response, the correction of the dose can be expressed as

$$D_m(p,E) = D_{\text{meas}} \cdot \frac{\overline{R}_{d,\text{calib}}}{\overline{R}_{\text{water,calib}}} \cdot \frac{\overline{R}_m(p,E)}{\overline{R}_d(p,E)} = D_d(p,E) \cdot \frac{\overline{R}_m(p,E)}{\overline{R}_d(p,E)}. \quad (1)$$

Here, a dose-in-material value D_m [Gy], as a function of the particles p and energies E in the radiation field, can be obtained by the application of two multiplicative correction factors to the measured dose D_{meas}: one for the correction of the calibration which results in the actual dose D_d deposited in the dosimeter material by the mixed-particle field and one to transform the dose to dose in one of the desired reference materials, water or air. The correction factors are composed of the ratio of the previously mentioned mean dose responses $\overline{R}$ (Gy $\cdot$ cm^2) of the materials to the mixed radiation field

$$\overline{R}_m(\text{MF}) = \frac{\sum_i \int \Phi_E(p_i,E) R_m(p_i,E)\, dE}{\sum_i \int \Phi_E(p_i,E)\, dE} \quad (2)$$

with this, the mean response of a material to the mixed radiation field can be determined by a convolution of the differential fluence $\Phi_E = (\partial\Phi/\partial E)$ (GeV^{-1} $\cdot$ cm^{-2}) of particle p with the response of the material in the particle field. The use of the response in (2) circumvents the necessity of time-intensive simulations of the specific irradiation situation for the dosimeter material and the reference material in the mixed radiation field. The necessary input for the correction is therefore reduced to the fluence of the field present during irradiation. In order to implement the mean response, energy response curves for selected energies in dosimeter material, water, and air considering the dimensions of the dosimeter were simulated in FLUKA for stable particles (γ, e$-$, e$+$, and p) in an energy range of 1 keV–10 TeV, for neutrons in an energy range of 10^{-5} eV–10 TeV, and for unstable particles (K$-$, K$+$, $\mu-$, $\mu+$, $\pi-$, and $\pi+$) in an energy range of 100 keV–10 TeV.

An example of an energy response curve can be found for neutrons in Fig. 5, and the peaks of this response curve can be attributed to the different elements present in the examined materials by comparing them with the neutron total cross section. For the case of the FD7 dosimeter material with a composition as stated in Table I, the total neutron cross section is shown in Fig. 6 with data from the Evaluated Nuclear Data File (ENDF) database [20], [21].

A verification of the previously introduced convolution of the differential fluence with the response of the material was performed by simulating conditions similar to the calibration irradiation conditions and an experiment where dosimeters were irradiated with a ^{60}Co source. Here, the calibration factors for the correction of the dose cancel out, but the dose deposited in the dosimeter material and water can be scored directly in FLUKA and can be compared with the calculated dose. Similar to (2), the dose can be determined by the convolution of the fluence and the response for all particle

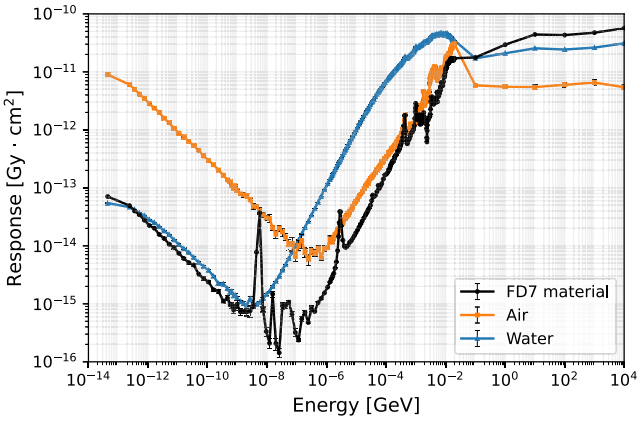

Fig. 5. Neutron energy response curve for dosimeter material, water and air the size of the dosimeter, used in the calculation of the mean response in the dose correction.

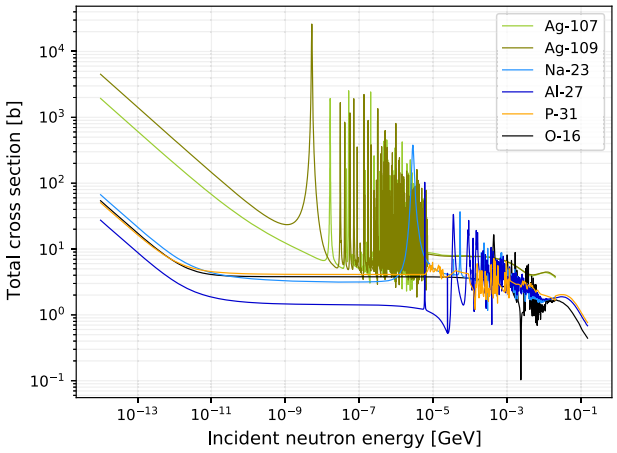

Fig. 6. Total neutron cross section for the individual elements in FD7 dosimeter material (composition, see Table I). Data from the ENDF database [20], [21].

types p in the following way:

$$D_m(\mathrm{MF}) = \sum_i \int \Phi_E(p_i, E) R_m(p_i, E)\, dE = \sum_i D_{m_i}. \quad (3)$$

In the calibration conditions, the dosimeters are enclosed in a 3-mm polymethyl methacrylate (PMMA) container; for this reason, the calibration radiation field contains electrons mainly due to Compton scattering in addition to photons. This is considered in the simulations by placing the dosimeters behind the PMMA plate of the same thickness, as shown in Fig. 7.

IV. Fading Effects

Although there is a good stability of the radiation-induced optical centers and a repeatable readout of the dosimeter is possible, these centers are subject to decay with time, the so-called fading effects, leading to an underestimation of the absorbed dose [10]. RPLDs have shown very slow fading effects, about 3%–10% per year depending on several factors such as the total integrated dose deposited in the dosimeter, ambient temperature in storage, exposure time, and the time after exposure (cooling time) [22]. However,

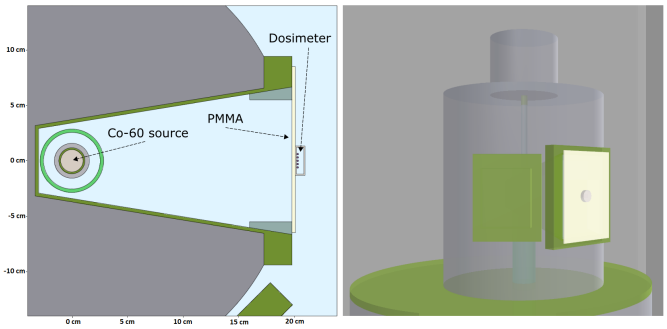

Fig. 7. Horizontal cross section and perspective view of the dosimeter irradiation setup used in the simulation of the irradiation experiment, dosimeters are placed behind the PMMA plate.

TABLE II
Fading Parameters for the RPL Centers Used in the Biexponential Fit Function in Fig. 8

Dose [Gy]	$C_{1,0}$ **[arb. unit]**	$1/\lambda_{C,1}$ **[days]**	$C_{2,0}$ **[arb. unit]**	$1/\lambda_{C,2}$ **[days]**
10	4.44	6.08	$9.39 \cdot 10^{-1}$	$1.41 \cdot 10^{4}$

in the RadMON activity at CERN, they are used under long exposure and cooling times, i.e., about one year comprising the LHC physics runs and about one year for the readout measurement constrained by accessibility and the retrieval of the dosimeters. Although the fading effects can be considered negligible for several applications, in the accelerator context, it is important to estimate and correct the readout of faded dosimeters. The fading speed is governed by the decay time of each type of optical center and it was shown that at least two different types for RPL and color centers, respectively, dominate the fading effects [8], [23], [24]. Each of these centers presents a different decay rate that strongly depends on the temperature and exposure to ambient light. However, at CERN, the irradiated dosimeters are kept in a climate chamber where the temperature, humidity, and light conditions are closely monitored. Also, when in the accelerator environment, the ambient temperature is between 15 °C and 20 °C, in which, in our previous studies, the temperature effect has shown to be negligible. Therefore, the decay velocity of each center type can be assumed to be constant over time. Accordingly, a correction procedure has been developed at CERN to quantify the fading response of the dosimeters by using a biexponential decay function for both RPL and color centers [12]

$$C(t) = C_{1,0} \cdot e^{-\lambda_{C,1} \cdot t} + C_{2,0} \cdot e^{-\lambda_{C,2} \cdot t} \quad (4)$$

where $C(t)$ is the total number of optical centers (either RPL or color centers) as a function of time t, $C_{1,0}$ and $C_{2,0}$ are the optical center density at $t = 0$ for each type of center, and $\lambda_{C,1}$ and $\lambda_{C,2}$ are their corresponding decay constants.

The reduction of the center density can be correlated experimentally with the light intensity measurement of the RPL light and the transmission light. For color centers, their decay leads to an increased transmittance of the blue transmission light through the RPLD, which leads to an increased measured signal and, therefore, a reduction of the measured dose. A faded measured dose would therefore be underestimated

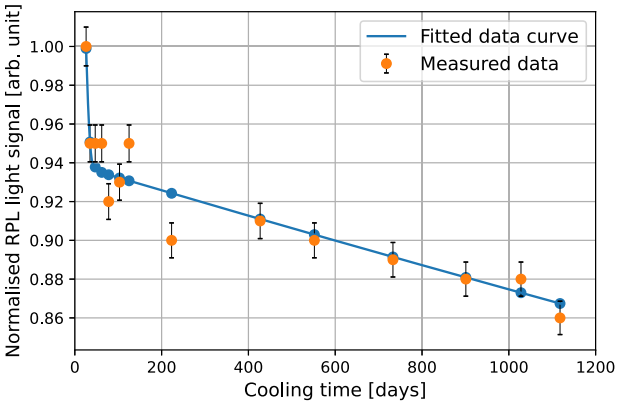

Fig. 8. Normalized signal of dose measurements for a dosimeter irradiated to 10 Gy and measured for 1118 days. The orange curve represents the measured data points and the blue curve shows the biexponential fitted data points.

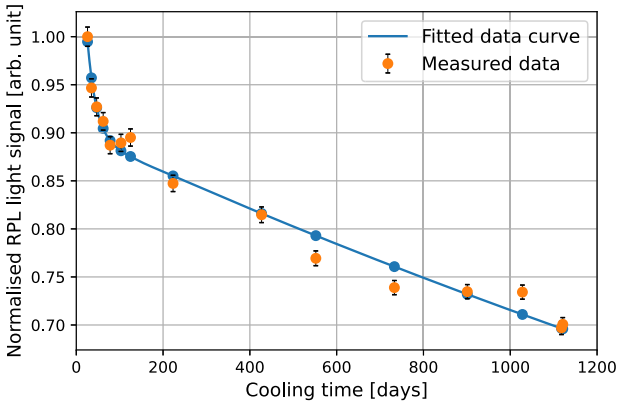

Fig. 9. Normalized signal of dose measurements for a dosimeter irradiated to 1 kGy and measured for 1121 days. The orange curve represents the measured data points and the blue curve shows the biexponential fitted data points.

TABLE III

FADING PARAMETERS FOR THE COLOR CENTERS USED IN THE BIEXPONENTIAL FIT FUNCTION IN FIG. 9

Dose [Gy]	$C_{1,0}$ **[arb. unit]**	$1/\lambda_{C,1}$ **[days]**	$C_{2,0}$ **[arb. unit]**	$1/\lambda_{C,2}$ **[days]**
1000	$3.58 \cdot 10^2$	$2.04 \cdot 10^1$	$9.00 \cdot 10^2$	$4.36 \cdot 10^3$

TABLE IV

VERIFICATION OF THE RESPONSE CONVOLUTION

Type	**Material**	**Dose per primary** 10^{-5}**[Gy]**	**Dose [Gy]**
Simulated	FD7	1.67(2)	92 ± 4
	Water	1.87(2)	102 ± 4
Calculated	FD7	1.694(2)	93 ± 3
	Water	1.953(4)	107 ± 3
Measured	Water eq.		102 ± 3

by a measurement with the transmission light. The situation for RPL light fading is more complicated, as in this case there exists a combined effect of the fading of the RPL centers and the color centers. Because of the presence of color centers, the production of RPL photons in the dosimeter is decreased: for one, due to the absorption of incoming UV light used for the excitation of the RPL centers, and for another, due to the absorption of the produced photons. As a consequence, the emitted RPL light is decreased by the decay of the RPL centers and increased by the decay of the color centers. For this reason, the behavior of the RPL light output, and therefore the measured signal, with fading is not always decreasing but can even increase in higher dose regions (>3 kGy) [12]. The fading of the centers is therefore dependent on the absorbed dose and the calculation of the fit values needs to be performed for each of the calibration dose values. For that, measurement data of the reference dosimeters were recorded for different timescales considering the expected *in situ* time and cooling time of the dosimeters that are used. In Fig. 8, an example for the fading of the RPL centers with time is presented. Here, the RPL light signal for a dosimeter irradiated with a dose of 10 Gy was measured for 1118 days and normalized to the initial measurement, and with the biexponential fit described in (4), an RPL center fading function could be found. The parameters of the fit in Fig. 8 are shown in Table II. An equivalent measurement and fit example for color center fading is shown in Fig. 9 and Table III, where a dosimeter with a received dose of 1 kGy was examined for 1121 days.

V. RESULTS

A. Mixed-Particle Response

In Table IV, the data to the verification of the response approach for mixed radiation fields can be found. Simulated and calculated values are given in dose per primary of the FLUKA simulation. As the simulation was conducted with radioactive decay of a ^{60}Co source, it refers to the decay of one radioisotope. For a comparison to the experimentally achieved and measured dose, the dose per primary value can therefore be calculated with the 5.19(8)-TBq activity of the source and the 10 540(120)-s time in irradiation. The dose was once simulated directly in FLUKA by scoring the dose deposited in the dosimeter material and by calculating the dose by the convolution of the particle field scored in vacuum with the response. A good accordance of the values within the 1σ uncertainty could be found for the simulated, the calculated, and the measured values. Here, the measured dose must be interpreted as water equivalent dose and compared directly with the simulation and calculation of dose deposited in water, as the conditions in this irradiation experiment are comparable to the calibration irradiation of the dosimeters.

With the simulated and calculated data achieved in the simulations of the ^{60}Co source, the correction factor for the calibration of the dosimeter R_d/R_W [see (1)] was determined. The simulated factor is 0.894 ± 0.012 and the calculated 0.867 ± 0.002. As the simulated correction factor is without the additional convolution with the response, this value is used for the correction of the dose. The necessity of the dose correction can be illustrated with exemplary radiation fields that are simulated to resemble the conditions in the SPS. The radiation fields are caused by a 400-GeV/c proton beam hitting an iron target. In two cases, the impact area is enclosed by a bulk material consisting of iron to describe beam losses in a massive magnet.

The scored regions can be seen in Fig. 10 and the results for the correction factor to the radiation field and the resulting

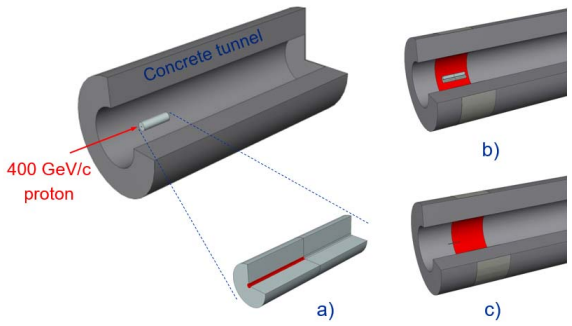

Fig. 10. Position of the scoring of exemplary radiation fields caused by a 400-GeV/c proton beam to an iron target. Radiation field in (a) iron target surrounded by iron bulk material, (b) close to concrete wall with bulk material, and (c) close to concrete wall without bulk material.

TABLE V

DOSE CORRECTION FACTOR FOR EXEMPLARY FIELDS IN THE SPS

Position	$\frac{R_{Water}}{R_d}$	$\frac{R_{Air}}{R_d}$	Dose correction factor	
			Water	Air
Beam impact area	1.2051(6)	0.8333(5)	1.08(2)	0.75(1)
At concrete wall situation b)	3.687(2)	1.515(2)	3.30(5)	1.36(2)
At concrete wall situation c)	1.2664(6)	0.7820(6)	1.13(2)	0.70(1)

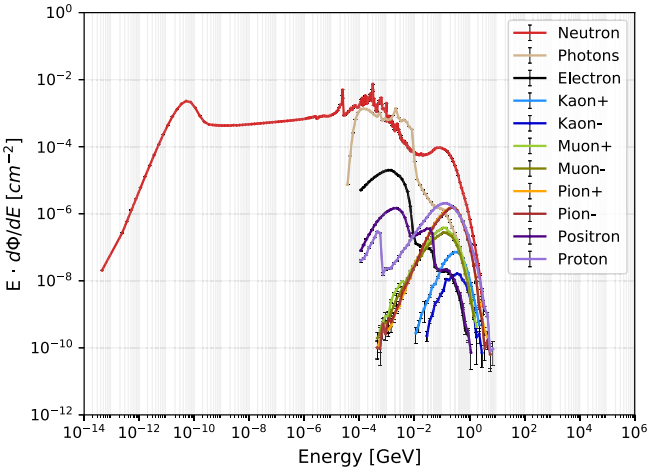

Fig. 11. Lethargy plot of the fluence spectrum of the mixed-particle field in situation (b) shown in Fig. 10, close to the concrete tunnel wall with a massive iron substitute surrounding the target.

correction factor to the dose according to (1) can be found in Table V.

As one can see in Table V, the absorbed dose referenced to dose to water can deviate significantly from the dose deposited in air for mixed-particle fields. This discrepancy is most prominent in radiation fields dominated by neutrons with an energy up to 20 MeV, as is the case for the position shown in Fig. 10(b). Comparing the fluence spectra of the mixed field in situation (b) in Fig. 11 and (c) in Fig. 12 shows the abundance of neutrons in the previously mentioned energy region for situation (b) with iron surrounding the beam impact region due to secondary particle interactions. The reason behind the high response of water to neutrons, which can be seen in the simulated neutron energy response curve in Fig. 5, is the high neutron scattering cross section of hydrogen

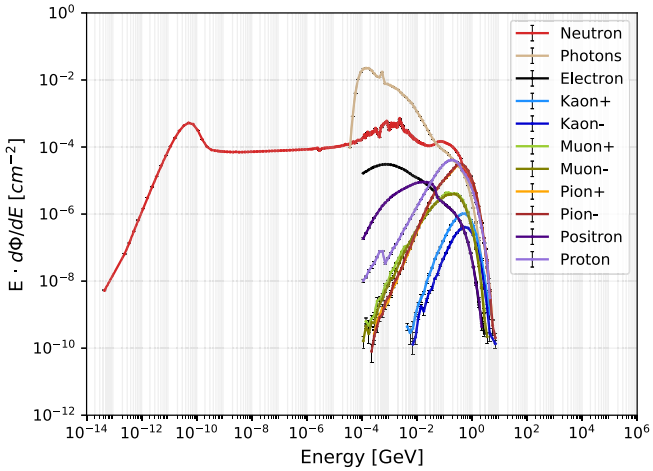

Fig. 12. Lethargy plot of the fluence spectrum of the mixed-particle field in situation (c) shown in Fig. 10, close to the concrete tunnel wall.

and the high-energy deposition by elastic scattering due to the similar mass of neutrons and the proton in the nuclei of hydrogen.

B. Fading Effect

Finally, the fading correction was applied to a set of faded dosimeters irradiated in a ^{60}Co gamma field and it is shown together with the calibration curve and the fading corrected curve in Fig. 13. The corresponding reference dose, the faded measured dose, and the fading corrected dose of this measurement can be found in Table VI. These dosimeters correspond to the three different dose ranges observed in Fig. 2. Therefore, it is possible to analyze the different relationships between the fading of the RPL centers and the color centers. One can see that the fading of the color centers, and therefore the increase of the transmission signal, is more prominent than that of the RPL centers. This can be attributed to the previously mentioned situation for the case of the RPL light fading where the fading of the RPL and the color centers with opposing effects on the emission of RPL light must be regarded for.

Overall, with the exception of one dosimeter, the underestimation of the dose was observed in the faded dosimeters. The overestimation of the faded dosimeter occurs at a high dose of 100 kGy where the fading of the color centers is more pronounced than the fading of the RPL centers. The greatest fading effect was identified for the readout measurements based on the transmission light where the decay time of the color centers dominates.

In Table VI, the reference value and the faded measured and corrected dose values are presented along with their respective percentage difference. The impact of fading can lead to a difference in the measured dose from 0.1 to about 44%. The lowest fading effect was observed for the dosimeter with a reference dose of 56.2 kGy that corresponds to the high-dose range where the fading of both RPL and color centers counteract each other. These RPLDs were stored for approximately five years (1833 days) in a controllable temperature and humidity environment, and however, the maximum correction value validated in this methodology was limited to 1500 days. Despite this limitation, by adopting the fading

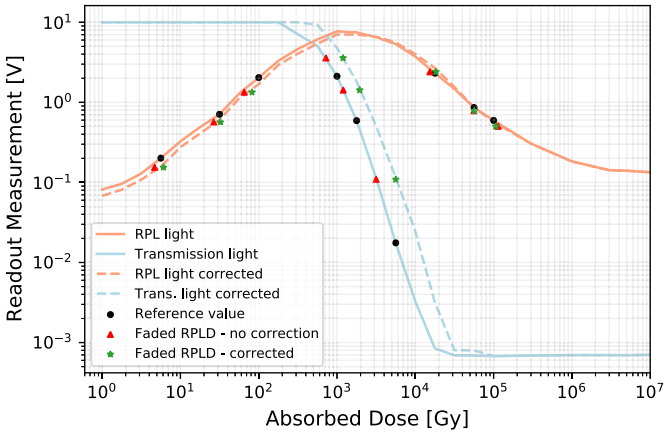

Fig. 13. Nominal and corrected calibration curve for the RPL and transmission light. Reference data points (black circles) for the faded dosimeters and measurements without correction (red triangles) and with correction (green stars). Fading time of approximately five years (1833 days).

TABLE VI

REFERENCE DOSE, FADED MEASURED DOSE, AND THE CORRECTED MEASURED DOSE

Reference Dose [Gy]	Faded Measured Dose [Gy]	Corrected Measured Dose [Gy]
5.6	4.7 (-16.7%)	6.1 (8.1%)
31.6	26.6 (-15.7%)	32.4 (2.6%)
100	65.3 (-34.7%)	82.3 (-17.7%)
1000	722.5 (-27.7%)	1194.7 (19.5%)
1780	1202.0 (-32.5%)	1951.8 (9.7%)
5620	3159.4 (-43.8%)	5629.1 (0.2%)
17800	15362.8 (-13.7%)	18313.1 (2.9%)
56200	56136.5 (-0.1%)	56819.7 (1.1%)
100000	114365.4 (14.4%)	106391.2 (6.4%)

* The difference to the reference dose values is given in percentage for the faded measured dose and corrected measured dose.

correction, an improvement up to about 44% is observed in the measurement of the faded RPLDs.

VI. CONCLUSION

Radiation dosimetry is of utmost importance for the characterization of different environments ranging from medical applications to high-energy particle accelerators. For example, radiation-level monitoring is used as a tool to prevent radiation damage of electronic components and materials and therefore to improve the system lifetime in the LHC complex at CERN. In this context, the present work has presented a dosimetry system based on the RPLDs to measure the radiation levels in high-energy and mixed-particle fields. The fundamental mechanisms for the characterization of such dosimeters in such environments were also presented by taking into consideration the different particle response and the fading effects. A methodology to obtain the corrected dose values considering the dosimeter response in a mixed radiation field is proposed. In addition, to cope with the long irradiation times constrained but the operational runs of the accelerators and also the long storage time prior to the readout measurement of such passive dosimeters, the fading correction methodology developed and adopted at CERN is also presented.

REFERENCES

[1] Y. Q. Aguiar *et al.*, "Radiation to electronics impact on CERN LHC operation: Run 2 overview and HL-LHC outlook," in *Proc. 12th Int. Part. Accel. Conf.*, Campinas, Brazil, Aug. 2021, pp. 80–83.
[2] K. Bilko *et al.*, "Radiation environment in the LHC arc sections during run 2 and future HL-LHC operations," *IEEE Trans. Nucl. Sci.*, vol. 67, no. 7, pp. 1682–1690, Jul. 2020.
[3] G. Spiezia *et al.*, "The LHC radiation monitoring system—RadMon," *Proc. Sci.*, vol. 143, pp. 1–12, Jul. 2011.
[4] D. Di Francesca *et al.*, "Dosimetry mapping of mixed-field radiation environment through combined distributed optical fiber sensing and FLUKA simulation," *IEEE Trans. Nucl. Sci.*, vol. 66, no. 1, pp. 299–305, Jan. 2019.
[5] *FLUKA Website*. Accessed: Mar. 10, 2022. [Online]. Available: https://fluka.cern
[6] G. Battistoni *et al.*, "Overview of the FLUKA code," *Ann. Nucl. Energy*, vol. 82, pp. 10–18, Aug. 2015.
[7] T. T. Böhlen *et al.*, "The FLUKA code: Developments and challenges for high energy and medical applications," *Nucl. Data Sheets*, vol. 120, pp. 211–214, Apr. 2014.
[8] T. Yamamoto, Y. Yanagida-Miyamoto, T. Iida, and H. Nanto, "Current status and future prospect of RPL glass dosimeter," *Radiat. Meas.*, vol. 136, Aug. 2020, Art. no. 106363.
[9] H. Vincke and J. Trummer, "Response functions of radio-photo-luminescence and alanine dosimeters to various particle fields," CERN, Geneva, Switzerland, Tech. Note, EDMS 2592261, 2021.
[10] K. Becker, *Solid State Dosimetry*, vol. 141. Boca Raton, FL, USA: CRC Press, 1973.
[11] F. Ravotti, "Dosimetry techniques and radiation test facilities for total ionizing dose testing," *IEEE Trans. Nucl. Sci.*, vol. 65, no. 8, pp. 1440–1464, Aug. 2018.
[12] H. Vincke and J. Trummer, "Fading correction for CERN's high-level dosimetry radio-photo-luminescence readout device," CERN, Geneva, Switzerland, Tech. Note, EDMS 2248808, 2020.
[13] L. BØtter-Jensen, "Luminescence techniques: Instrumentation and methods," *Radiat. Meas.*, vol. 27, nos. 5–6, pp. 749–768, Dec. 1997.
[14] H. Schonbacher, M. Furstner, and H. Vincke, "High-level dosimetric methods," *Radiat. Protection Dosimetry*, vol. 137, nos. 1–2, pp. 83–93, Nov. 2009.
[15] C. R. Ronda, *Luminescence: From Theory to Applications*. Hoboken, NJ, USA: Wiley, 2007.
[16] J. Trummer, "Characterisation of CERN's high level dosimetry radio-photo-luminescence readout system," CERN, Geneva, Switzerland, Tech. Note, EDMS 2275199, 2020.
[17] A. Brynjolfsson and N. Holm, "The Co 60 irradiation facility and the gamma field at Risø," in *Large Radiation Sources in Industry*. Salzburg, Austria: IAEA, 1960.
[18] H. Vincke and J. Trummer, "Apparatus and method for determining a dose of ionizing radiation," WO Patent 2 014 161 732, Feb. 2016.
[19] D. Pramberger *et al.*, "Radio-photo luminescence measurement dose correction for arbitrary mixed radiation fields," CERN, Geneva, Switzerland, Tech. Note, EDMS 2599921S, 2021.
[20] *Evaluated Nuclear Data File (ENDF) Website*. Accessed: Mar. 10, 2022. [Online]. Available: https://www-nds.iaea.org/exfor/endf.htm
[21] D. Brown *et al.*, "ENDF/B-VIII.0: The 8th major release of the nuclear reaction data library with CIELO-project cross sections, new standards and thermal scattering data," *Nucl. Data Sheets*, vol. 148, pp. 1–142, 2018.
[22] F. Coninckx, H. Schönbacher, M. Tavlet, G. Paic, and D. Razem, "Comparison of high-dose dosimetry systems for radiation damage studies in collider detectors and accelerators," *Nucl. Instrum. Methods Phys. Res. Sect. B, Beam Interact. With Mater. At.*, vol. 83, nos. 1–2, pp. 181–188, Oct. 1993.
[23] S. W. S. McKeever, S. Sholom, N. Shrestha, and D. M. Klein, "Build-up of radiophotoluminescence (RPL) in Ag-doped phosphate glass in real-time both during and after exposure to ionizing radiation: A proposed model," *Radiat. Meas.*, vol. 132, Mar. 2020, Art. no. 106246.
[24] K. Farah *et al.*, "Characterization of a silicate glass as a high dose dosimeter," *Nucl. Instrum. Methods Phys. Res. A, Accel. Spectrom. Detect. Assoc. Equip.*, vol. 614, no. 1, pp. 137–144, Feb. 2010.